Hindawi
International Journal of Aerospace Engineering
Volume 2024, Article ID 4340688, 13 pages
https://doi.org/10.1155/2024/4340688

Research Article

Numerical Investigation on the Effect of Fuel-Rich Degree in the RBCC Engine under the Ejector Mode

Yizhi Yao, Mingbo Sun, Menglei Li, Peibo Li, An Bin, Rui Gu, Jiaoru Wang, Feng Wei, Taiyu Wang, and Jikai Chen

Science and Technology on Scramjet Laboratory, College of Aerospace Science and Engineering, National University of Defense Technology, Changsha, Hunan 410073, China

Correspondence should be addressed to Mingbo Sun; sunmingbo@nudt.edu.cn and Peibo Li; lipeibo09@nudt.edu.cn

Received 15 February 2023; Revised 18 July 2023; Accepted 16 October 2023; Published 6 February 2024

Academic Editor: Antonio Concilio

The ejector mode of the Rocket-Based Combined-Cycle (RBCC) engine is characterized by high fuel consumption. This study is aimed at investigating the influence of the rocket fuel-rich degree on the RBCC engine's performance under the ejector mode combined with simultaneous mixing and combustion (SMC). Numerical simulations were conducted for various rocket mixing ratios ($\Phi = 1.6 \sim 3.2$) under subsonic ($Ma_f = 0.9$) and supersonic ($Ma_f = 1.8$) flight conditions. It was observed that a high fuel-rich degree in the rocket plume negatively impacts the eject performance under all conditions. However, it improves the overall performance (I_{sp}) at high flight Mach numbers (Ma_f). For supersonic conditions, increasing the fuel-rich degree promotes greater fuel participation in combustion, thereby enhancing RBCC engine performance. Nevertheless, the subsonic-supersonic mixing layer exhibits low evolution, resulting in a decrease in reaction efficiency from 29.2% to 12.0% as the Φ decreases from 3.2 to 1.6. Consequently, there is an inefficient utilization of fuel. To optimize RBCC engine performance, the rocket fuel-rich degree can be appropriately increased. However, this increase should be limited to prevent fuel wastage arising from low reaction efficiency. Under subsonic conditions ($Ma_f = 0.9$), the low kinetic energy of captured air leads to the occurrence of "negative thrust surface" and "wall impact" phenomena, which hinder the efficient and stable operation of the RBCC engine. Consequently, adjusting the fuel-rich degree alone cannot promote specific impulse (I_{sp}), and a low fuel-rich degree is considered an ideal strategy when combined with adjustable nozzle technology.

1. Introduction

With the increasing prominence of economic challenges in the aerospace sector, the RBCC (Rocket-Based Combined Cycle) engine has garnered significant attention from scholars. The RBCC engine integrates a rocket engine with the inner flow channel of a ramjet engine, offering a synergistic combination of the high thrust-to-weight ratio of a rocket engine and the high specific impulse (I_{sp}) characteristic of an air-breathing engine [1–3]. Aircraft powered by the RBCC engine exhibit improved performance in terms of flight trajectory, acceleration, and cruise capabilities [4–6]. Additionally, these aircraft have the ability to take off and land horizontally, even from sea level, solely relying on the RBCC engine for space access [7, 8]. Owing to its high efficiency and reusability, the RBCC engine is recognized as one of the most promising propulsion systems available [9–11].

Generally, based on flight Mach number and altitude (H_f), RBCC engines can be categorized into ejector, ramjet, scramjet, and rocket modes [8]. It has been observed that fuel consumption during the climbing phase constitutes approximately 50% of the entire flight process, making the ejector mode particularly crucial during this phase [4, 12]. When Ma_f ranges from 0 to 2.5, the RBCC engine operates in the ejector mode, where the rocket plume expels air from the atmospheric environment. Work and Haedrich [13] proposed that the rocket plume acts as the driving force for capturing air in the ejector mode when the engine inlet is in a nonstart state, referred to as eject performance. The state

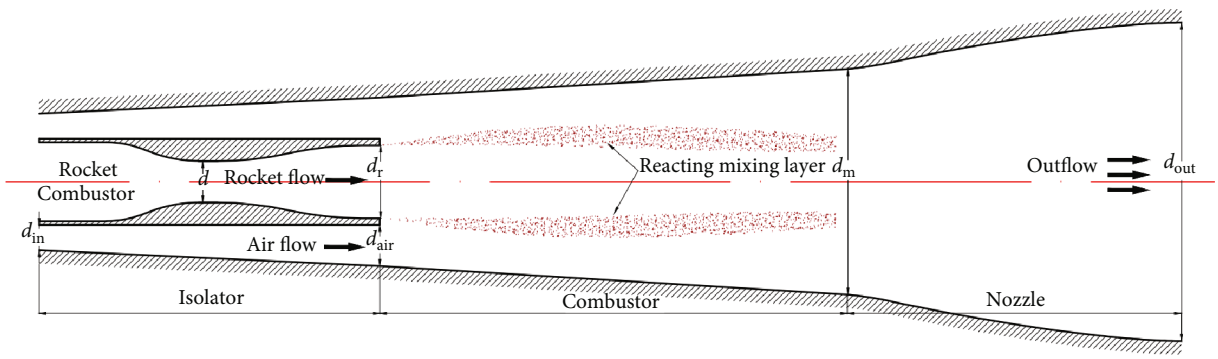

Figure 1: Schematic illustration of the RBCC engine.

of the rocket plume and its working parameters significantly impact the performance in the ejector mode [14]. The thrust of the RBCC engine is derived from two sources: rocket thrust and afterburning thrust. The fuel in the rocket plume reacts with the oxidant in the captured air, generating afterburning thrust in the combustor. However, the rocket plume, characterized by high temperature, high speed, and rich combustion, exhibits considerable compressibility and exothermic effects, leading to decreased mixing efficiency between the plume and the ambient air and hindering the reaction process [15, 16]. Consequently, adjusting the working conditions of the rocket to ensure optimal mixing and reaction efficiency has become an urgent key technology to be addressed, ultimately enhancing the overall performance of the RBCC engine.

Under the ejector mode, it is necessary to adjust the rocket's operating parameters according to the flight conditions [17] in order to improve overall performance while meeting thrust requirements. Parkinson et al. [18] asserted that the eject performance of the rocket plume increases with higher mixing ratios (Φ). Koupriyanov and Etele [19] discovered, using a quasi-one-dimensional thermodynamic model that eject performance is highly sensitive to mixing ratios (Φ). When the rocket plume is rich in fuel or oxygen, the eject performance is favorable; however, a fully-reacted plume results in minimal eject performance. Han et al. [20] conducted a comprehensive investigation into the impact of molecular weight (rocket plume) on the overall performance. The research findings indicate that with an increase in molecular weight, both the engine's injection performance and specific impulse performance demonstrate a gradual decrease. However, there is a simultaneous progressive increase in thrust and thrust gain. Petersen et al. [14] delved into the influence of the molar mass fraction of the rocket plume on ejector performance. Their study revealed that the eject performance of the RBCC engine primarily relies on the total pressure ratio and momentum exchange efficiency of the two flows. Furthermore, they observed that a higher molar mass fraction corresponded to a poorer eject performance.

Research on mixing ratios (Φ) primarily focuses on eject performance due to the difficulty in experimentally and theoretically obtaining flow characteristics in RBCC combustors. This paper utilizes CFD (computational fluid dynamics) technology to quantitatively analyze parameters such as react efficiency (η_R), specific impulse (I_{sp}), and wall pressure (P). This analysis aims to uncover the influence of Φ on the RBCC system under the ejector mode.

Table 1: Structural parameters of RBCC engine.

	d	l_2	d_{in}	d_{air}	d_m	d_{out}
Parameters	1	11.29	2.58	3.55	5.48	7.74

Table 2: The inlet and outlet configuration.

Condition	H/km	Ma	P/kPa	P_0/kPa	T/k	T_0/k
Subsonic	9.5	0.9	28.5	48.2	226.4	263.0
Supersonic	11.6	1.8	20.7	101.2	216.7	357.0

Table 3: The mass fraction of the rocket plume with different mixing ratios (Φ).

Φ	Mass fraction of $C_{12}H_{23}$	Mass fraction of CO_2	Mass fraction of H_2O
1.6	13.73%	61.96%	24.31%
2.0	9.80%	64.78%	25.42%
2.4	6.54%	67.12%	26.34%
2.8	3.77%	69.11%	27.12%
3.2	1.40%	70.81%	27.79%

2. Materials and Methods

2.1. Configuration of the RBCC Engine. In this paper, the axisymmetric configuration of the RBCC engine as shown in Figure 1 was used for analysis. This configuration was tested for ground performance in the science and technology on the scramjet laboratory of the National University of Defense Technology [21, 22]. The rocket is arranged in the central axis of the RBCC engine. After the high-temperature plume expands from the rocket nozzle, it enters the combustor of the RBCC engine, and the captured air also enters the combustor through the inlet and isolator. In the combustor, the fuel-rich rocket plume mixes and reacts with the captured air, called SMC (simultaneous mixing and

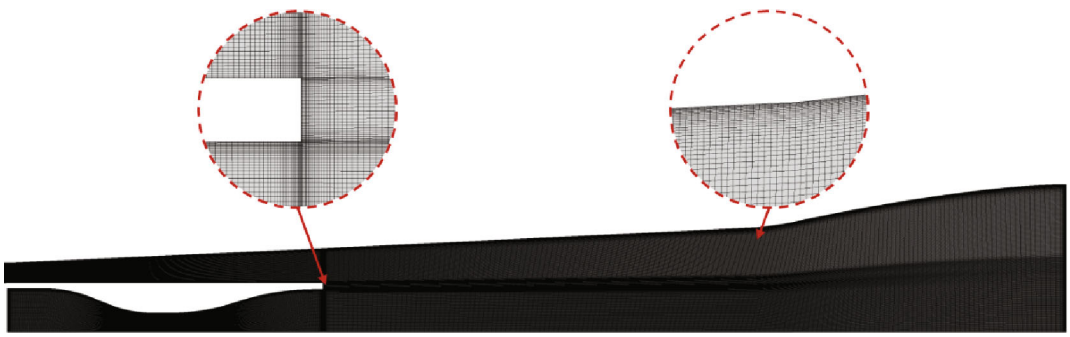

Figure 2: Schematic illustration of the grid model.

combustion). The reacting mixing layer in the combustor generates thrust and increases I_{sp}. Then, the mixed flow expands in the RBCC engine nozzle and is discharged from the RBCC engine through the nozzle outlet.

2.1.1. Configuration of the RBCC Engine. The dimension of the model is based on the rocket throat dimension (d). The specific dimensions are shown in Table 1, where the outlet diameter of the combustor (d_m) is 5.48 and the axis length of the combustor (l_2) is 11.29. The inlet and outlet conditions referred to the flight trajectory of Jia et al. [4]. The aircraft was released from the vehicle with $H_f = 9.5$ km and $Ma_f = 0.8$, and the ejector mode was designed as $Ma_f = 0.8 \sim 3.0$. In the CFD calculation, $Ma_f = 0.9$ and $Ma_f = 1.8$ were selected as the subsonic and supersonic flight conditions. Because the inlet of the RBCC engine was not started and the total pressure loss was very small, the effect of the inlet was ignored in the calculation, and the total pressure recovery coefficient of 0.95 was used to calculate the aerodynamic parameters of the isolator inlet. The configuration of the aerodynamic parameters of the isolator inlet and outlet of the RBCC engine is shown in Table 2.

2.1.2. Rocket Configuration. An O_2/kerosene rocket was embedded in the central axis of the RBCC engine. The operating parameters were set as follows: the total pressure (P_0) of the rocket was 3 MPa, the total temperature (T_0) was 3500 K, and the Mach number (Ma) of the plume at the rocket outlet was 2.8. The nozzle was designed by the characteristic line method. Φ refers to the ratio of the mass flow of kerosene and oxygen during rocket supply. In this paper, it was assumed that the rocket plume with different Φ conditions had fully reacted in the rocket combustion chamber, and the influence of Φ on the P_0 and T_0 was not considered, so the rocket plume consisted of CO_2, H_2O, and kerosene. Kerosene could be simplified as a single compound ($C_{12}H_{23}$); the mass fraction with different Φ conditions is shown in Table 3. When $\Phi = 3.2$ and 2.8, the mass fraction of $C_{12}H_{23}$ (M) was 1.40% and 3.77%, and the rocket worked under slightly fuel-rich conditions. When $\Phi = 2.4$, the plume was moderately fuel-rich. When $\Phi = 2.0$ and 1.6, the kerosene content was close to or more than 10%, and the plume was heavily fuel-rich.

2.2. Numerical Methods. The CFD calculation was performed by solving 2D Reynolds-averaged Navier-Stokes (RANS) equations for the ideal gas based on the finite volume method, and the ICEM was applied for grid meshing. Considering supersonic conditions, the solution formulation and flux scheme are solved using implicit and Roe-FDS types. Other details of the numerical simulation are as follows.

2.2.1. Grid Model and Boundary Conditions. The calculation grid is shown in Figure 2, and its number was 535 K. The grid model was a 2D axisymmetric model, and the assignment of axisymmetry was used for the CFD calculation The assumption implies that there are no circumferential gradients in the flow, but that there may be nonzero circumferential velocities. In the study of RBCC engines, Gu et al. have validated that 2D RNG methods were appropriate [21]. The results of the 2D and 3D RNG methods were validated through comparisons with the experimental data of Hall [23] in which the convective Mach number is about 0.962. The grid was refined at the region of the wall and react. The height of the bottom grid above the wall is 0.1 mm, with the wall treatment in the viscous model, so that the boundary layer could be well simulated. The maximum grid size in the whole area is less than 2 mm.

The pressure-inlet boundary condition was adopted for the rocket inlet, and the P_0 and T_0 were 3 MPa and 3500 K. The component mass fraction was set, as shown in Table 2. The rocket gas was assumed to have fully reacted, and no combustion area was set inside the rocket. The pressure-inlet boundary condition was adopted for the inlet of the isolator section, and the RBCC engine outlet was set as the pressure-outlet boundary condition. The P and T of them were set, as shown in Table 2. The stationary wall was adopted for all wall surfaces, considering thermal insulation and no-slip conditions.

In the RBCC engine, the grid-scale is related to the calculation accuracy of the mixing layer and reaction. Therefore, three grids with different scales consisting of the coarse grid (26.4 thousand), the moderate grid (53.1 thousand), and the refined grid (101.0 thousand) were selected for the grid independence analysis. The boundary layer grid near the walls was generated, and the first cell height of the wall is 0.01 mm so that $y+$ was less than 2.0 for all three

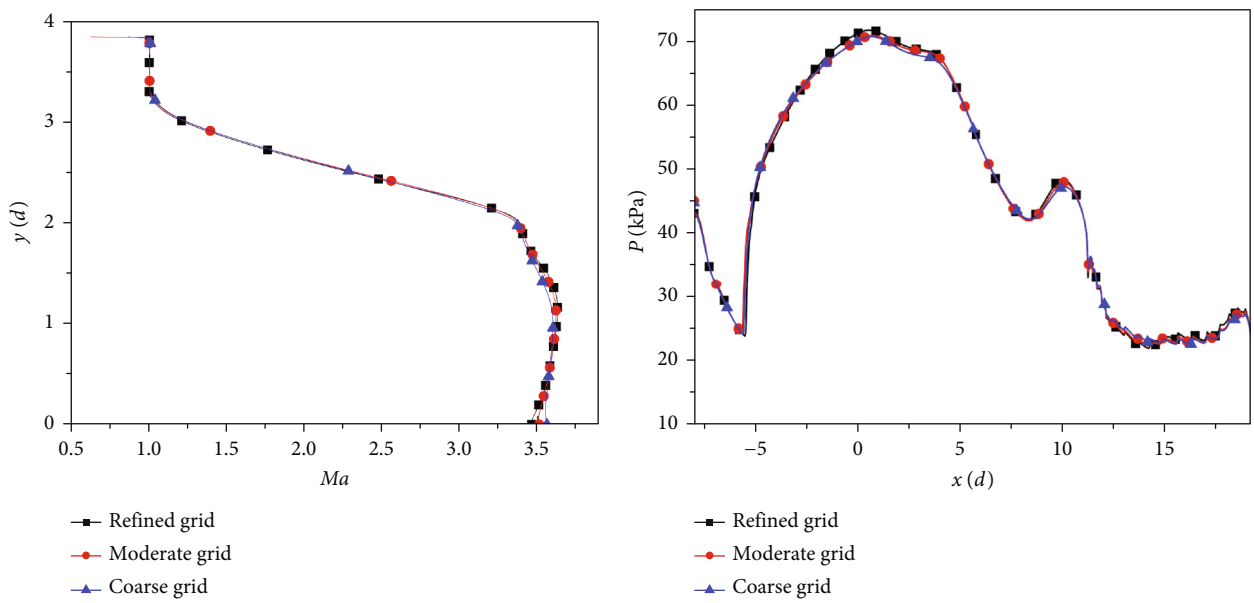

(a) Ma distribution at RBCC engine outlet

(b) P distribution along the x direction

Figure 3: Grid independence analysis image.

grids. Figure 3(a) shows that the outlet velocity profiles of the moderate and refined grids are consistent, while the coarse grid differs from others at the main flow ($y/d = 0 \sim 2.0$). Similarly, Figure 3(b) shows that the pressure distribution curves of the moderate and refined grids are consistent, while the pressure of the refined grid is slightly different in the combustor ($x/d = 0 \sim 5.0$). The grid independence analysis showed that the moderate grid satisfied the demand for numerical simulation, which was applied in this paper.

2.2.2. Viscous and Reaction Model. The RNG k - ε model was selected as the viscous model. The model was improved on the standard k - ε model, based on a mathematical technique called "renormalization group" (RNG) [5]. Compared with the standard k - ε model, the RNG model has an additional term in its equation that improves the accuracy for rapidly strained flows and could enhance the accuracy for swirling flows. So the RNG k - ε model was often used for numerical simulation of the mixing layer, which can meet the requirements of the CFD calculation about the RBCC engine under the ejector mode.

Enhanced wall treatment for k - ε model is a near-wall modeling method that combines a two-layer model with so-called enhanced wall functions. It could have a near-wall formulation that can be used with coarse meshes (usually referred to as wall-function meshes) as well as fine meshes (low-Reynolds number meshes) [6]. Therefore, it is more flexible in numerical calculation. When the mixing layer is highly compressible ($Mc > 0.6$), the compressibility effect should be considered [24]. For the mixing layer of rocket plume and air, compressibility affects turbulence through so-called "dilatation dissipation," neglected in

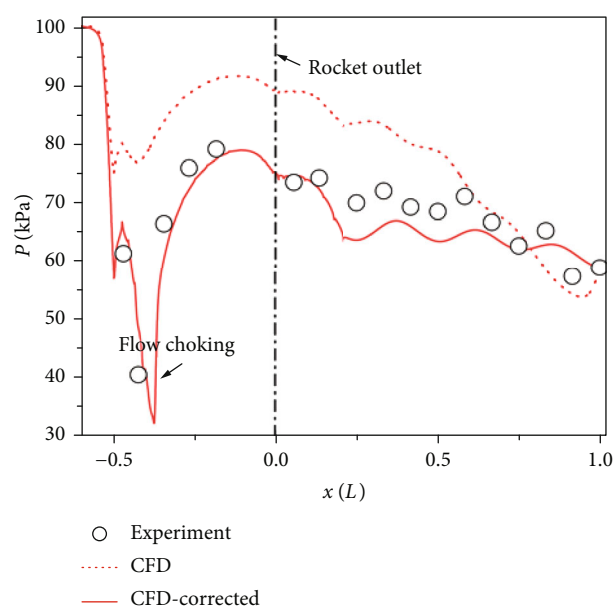

Figure 4: Pressure distribution contrast between CFD and experimental results.

incompressible flows. Therefore, the dilatation dissipation term (Y_M) was introduced for the k - ε model, namely,

$$Y_M = 2\rho\varepsilon M_t^2,$$
$$M_t = \sqrt{\frac{k}{a^2}}, \quad (1)$$
$$a = \sqrt{\gamma \mathrm{RT}},$$

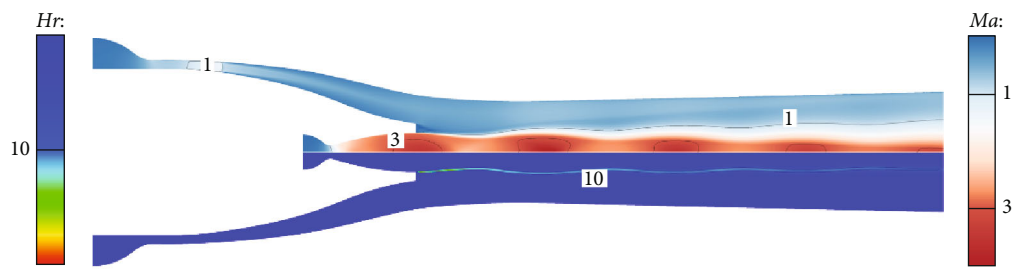

(a) The cloud chart of Ma and H_r with the compressibility effect

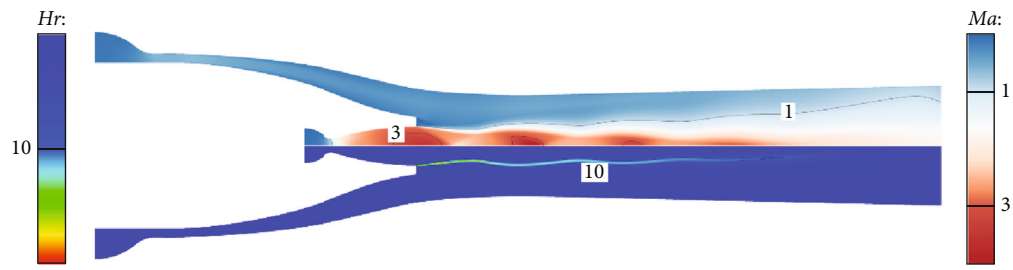

(b) The cloud chart of Ma and H_r without the compressibility effect

Figure 5: The CFD flow field with and without the compressibility effect.

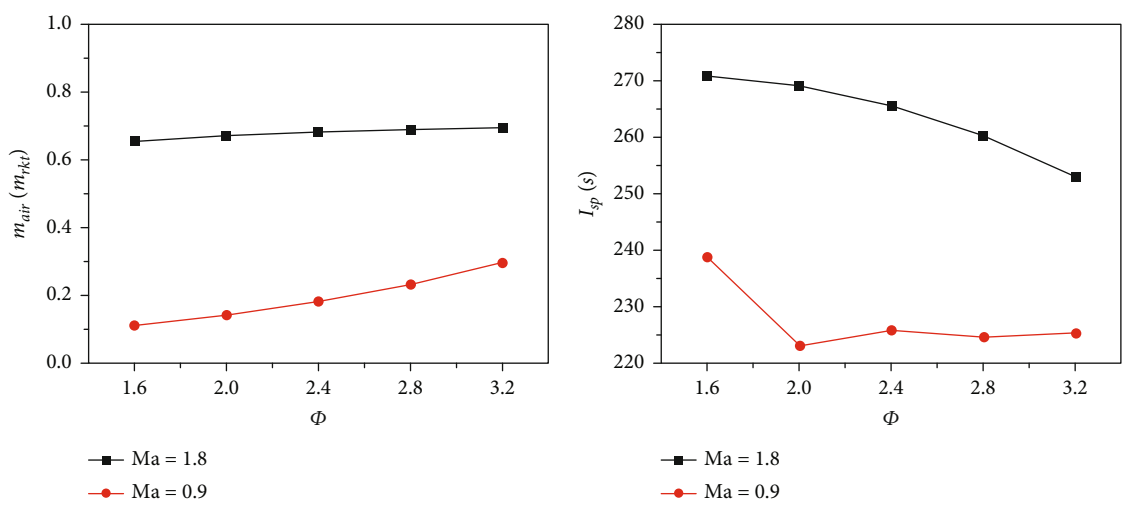

(a) Variation $\dot{m}_{air}/\dot{m}_{rkt}$ with Φ

(b) Variation of I_{sp} with Φ

Figure 6: System performance of the RBCC engine.

where M_t and a are the turbulent Mach number and speed of sound. Furthermore, k and ε are the turbulent kinetic energy and turbulent eddy dissipation. The Sarkar model has been tested for a very limited number of free shear test cases [25].

The one-step reaction mechanism was the chosen as reaction mechanism of calculation. The finite-rate/eddy-dissipation model was also chosen, and the reaction rates were first computed for each model separately (the finite-rate and eddy-dissipation model) and then the minimum of the two was used.

2.2.3. Numerical Validation. The one-step reaction mechanism and RNG k-ε model were used for the CFD calculation, and the experimental results of Gu et al. [21, 22] were chosen for numerical verification. The boundary conditions used for numerical simulation were experimental conditions, as shown below: the rocket inlet used pressure-inlet boundary condition, with $P_0 = 3.3$ MPa, $T_0 = 3400$ k, and the air inlet and outlet of the RBCC engine used the pressure-inlet and pressure-outlet boundary conditions. Figure 4 shows the contrast between the experiment and numerical simulation results. The abscissa is the standardized x-axis coordinate, and the ordinate is the wall pressure. It could be found that the wall pressure along the way obtained by considering the compressibility effect (shown as the CFD-corrected curve) corresponds well with the experiment results and can better reflect the flow choking in the isolator and the pressure in the combustor. However, without considering the compressibility effect (shown as the CFD curve), the wall pressure near

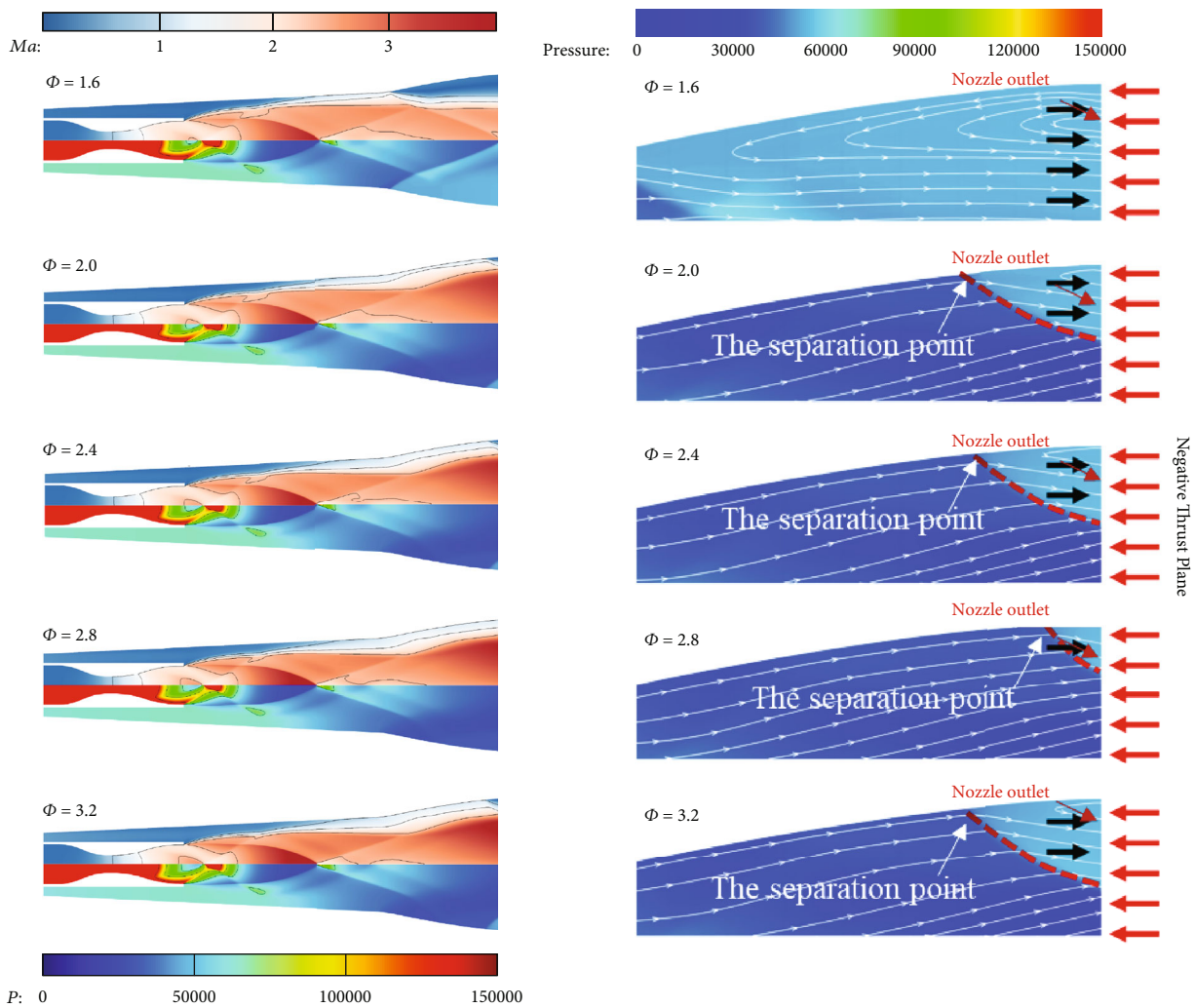

(a) The cloud chart of Ma and P with different Φ conditions

(b) The cloud chart of P and streamline with different Φ conditions

Figure 7: The cloud chart of Ma, P, and streamline ($Ma_f = 0.9$).

the rocket outlet was higher than the experiment results, and the pressure in the isolator rised without flow choking.

The numerical simulation flow field with and without the compressibility effect is shown in Figure 5. Figure 5(a) shows that when the compressibility effect was considered, the flow choking with $Ma = 1$ occurred in the isolator. However, when the compressibility effect was not considered (shown in Figure 5(b)), the flow in the isolator was subsonic flow with $Ma < 1$, which corresponded to the wall distribution results shown in Figure 4. The cloud chart of the reaction heat release (H_r) shows that the heat release area was large and the react intensity was high in the front section of the combustor because the compressibility effect was not considered. Without the compressibility effect, the evolution of mixing layers would be overestimated, so that the reaction intensity and area in the early stage of the reacting mixing layer could exceed the true value, causing the pressure in the combustor to rise, and the pressure would be transmitted back to the isolator, resulting in the inconsistency between the CFD and experiment results. It was clear that the compressibility effect should be used to revise the simulation to truly reflect the combustion and flow field in the RBCC engine.

3. Results and Discussion

3.1. Performance Analysis of the RBCC Engine. For RBCC engines, the specific impulse (I_{sp}) and the mass flow of captured air ($\dot{m}_{air}$) are the key indicators, which represent the basic performance of air-breathing propulsion systems. In this paper, the net specific impulse of the internal flow channel is used as the performance index, called I_{sp}. I_{sp} considers the performance of the rocket plume and reaction heat release, which is the propulsion performance of the entire RBCC engine, namely,

$$I_{sp} = \frac{\int_{out}\{\rho u|u| + (P - P_a)\}dA - \int_{in}\{\rho u|u| + (P - P_a)\}dA}{\dot{m}_{rkt}}, \tag{2}$$

where out and in are the outlet and inlet of the RBCC engine. ρ, u, and P are the local density, axial velocity, and pressure, respectively, what is more, P_a and $\dot{m}_{rkt}$ are ambient pressure and rocket mass flow, respectively. The mass flow of captured air determines the upper limit of oxidant that can participate in the reaction, which can measure the eject performance of RBCC engines under the ejector mode, called $\dot{m}_{air}$. $\dot{m}_{air}/\dot{m}_{rkt}$ is the eject performance index adopted after standardized analysis.

Figure 6 shows the change of the I_{sp} and capture air flow ($\dot{m}_{air}/\dot{m}_{rkt}$) with rocket mixing ratios (Φ), under Ma_f are 0.9 and 1.8. Under $Ma_f = 1.8$ condition, with the increase of Φ, the flow of captured air basically remains unchanged. At this time, the captured air has a certain kinetic energy and $\dot{m}_{air}/\dot{m}_{rkt}$ is not affected by the change of Φ. However, under $Ma_f = 0.9$ condition, with the increase of Φ, $\dot{m}_{air}/\dot{m}_{rkt}$ has a relatively significant increase. It indicates that the captured air kinetic energy is too small, which would be affected by Φ. Under subsonic flight conditions, Φ of the plume could affect the eject performance of RBCC engines, while under supersonic flight conditions, eject performance is not sensitive to the Φ.

The curves of I_{sp} with Φ are shown in Figure 6(b). When $\Phi = 3.2$, I_{sp} are 225.2 s and 252.8 s under $Ma_f = 0.9$ and 1.8 conditions. When $Ma_f = 0.9$, with an increase of Φ, $\dot{m}_{air}/\dot{m}_{rkt}$ has a relatively obvious increase, but I_{sp} has no significant change rule. Conversely, with $\Phi = 1.6$, although $\dot{m}_{air}/\dot{m}_{rkt}$ is the lowest, the I_{sp} of the RBCC engine is the highest, which shows that the performance of the RBCC engine is not only limited to the captured air but also closely related to other factors. The reasons would be analyzed later. When $Ma_f = 1.8$, the I_{sp} shows an upward trend with a decrease of Φ. However, with the decrease of Φ, the change range of I_{sp} (ΔI_{sp}) decreases, indicating that some factors are inhibiting the gain of I_{sp}, and the increased fuel cannot be fully converted into engine performance improvement.

3.2. Flow Characteristics under the Subsonic Condition

3.2.1. Analysis of Specific Impulse Loss. It is found that under low Ma_f conditions, in different Φ cases (except $\Phi = 1.6$), I_{sp} remains at a low level ($I_{sp} = 223.0 \sim 225.7$ s). In order to analyze the cause of I_{sp} loss, the cloud charts of Ma and P are shown in Figure 7(a). It could be observed from the figure that due to the low mass flow of the captured air, there is no shock in the isolator. When $\Phi = 2.0 \sim 3.2$, oblique shock waves appear in the RBCC nozzle. However, when $\Phi = 1.6$, the oblique shock wave is pushed forward to the outlet of the combustor chamber. Figure 7(b) shows the cloud chart of the streamline and P of the RBCC nozzle. At $\Phi = 2.0 \sim 3.2$, the flow separation occurs in the mixed flow behind the point of the oblique shock wave, and at $\Phi = 2.0$, 2.4, and 3.2, the flow separation even causes backflow at the rear of the nozzle. When $\Phi = 1.6$, the area of the backflow zone is expanded to the entire nozzle. With the decrease of Φ, the high fuel-rich degree in the plume inhibits the ejector performance. The low $\dot{m}_{air}/\dot{m}_{rkt}$ and kinetic energy of captured air are the main reasons for the flow separation in the nozzle. Interestingly, the flow separation in the nozzle makes RBCC performance rise instead of decline, which will be further analyzed.

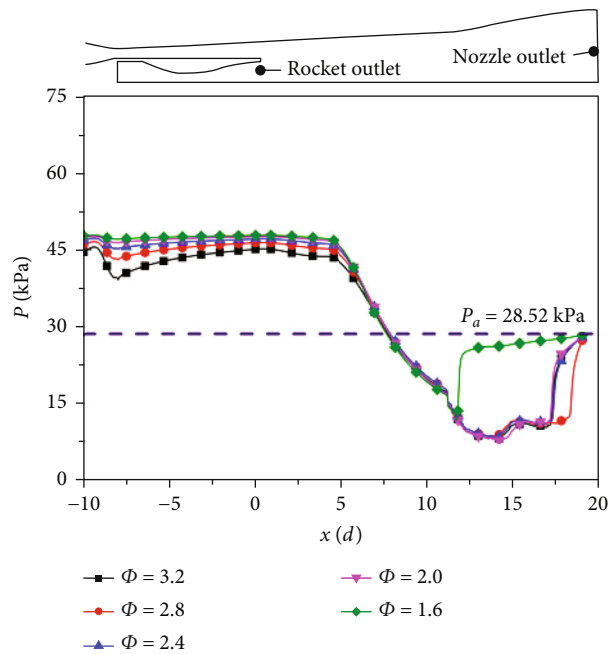

Figure 8: Pressure distribution with different Φ conditions ($Ma_f = 0.9$).

Figure 8 shows the wall pressure distribution of the RBCC engine. When $\Phi = 1.6$, the pressure rises at $x/d = 11.8$, which corresponds to the flow separation point, and then the wall pressure rises to the same value as P_a (28.52 kPa). When $\Phi = 2.0$, 2.4, and 3.2, the pressure rise point is $x/d = 17.2$, and when $\Phi = 2.8$, the pressure rise point moves to $x/d = 18.3$, and the fluid is discharged from the nozzle at the outlet before the backflow is formed. In the RBCC combustor and nozzle, the wall pressure in a large area is lower than P_a, and these surfaces would cause thrust loss, which is called "the negative thrust surface." When $\Phi = 1.6$, because of the large backflow zone, the pressure on the inner wall of the nozzle is higher than in other cases, which reduces the I_{sp} loss.

Under subsonic conditions, P_0 of the captured air is low. On the one hand, with the low kinetic energy of captured air, the corresponding combustion effect is poor, and on the other hand, the mass flow of the captured air is less, restricting the reaction in the mixing layer. Therefore, no matter how Φ changes, the RBCC nozzle cannot typically work because the pressure is lower than the ambient pressure, resulting in a "negative thrust effect." At this time, the backflow zone can reduce the "negative thrust surface." Therefore, when $\Phi = 1.6$, the large backflow zone generated has a significant positive impact on I_{sp}. Although the thrust loss is reduced when Φ is low, there is no effective thrust gain compared with the pure rocket without afterburn. Therefore, in order to give consideration to the performance under subsonic conditions, the ideal state is to realize the dynamic adjustment of the intake and exhaust system when designing the RBCC engine nozzle. Through structural adjustment, the "negative thrust effect" phenomenon can be avoided.

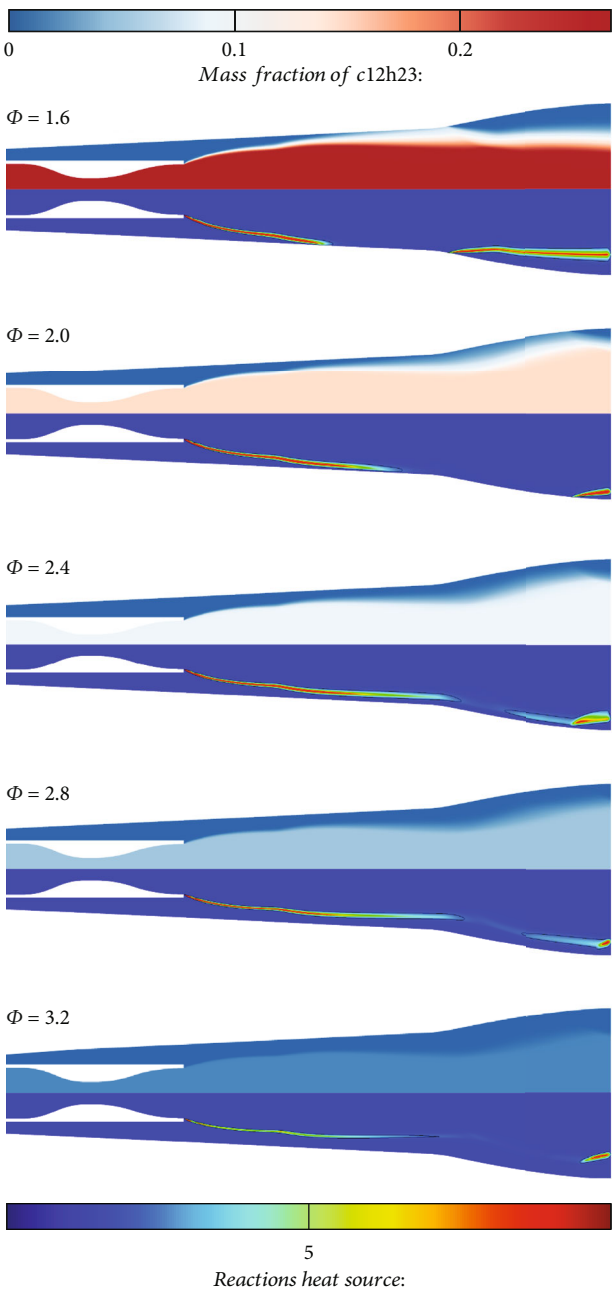

Figure 9: The cloud chart of M and H_r with different Φ conditions ($Ma_f = 0.9$).

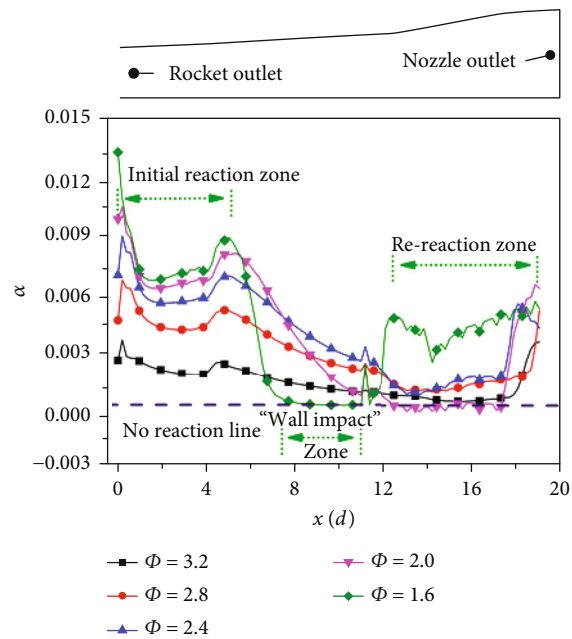

Figure 10: α distribution with different Φ conditions ($Ma_f = 0.9$).

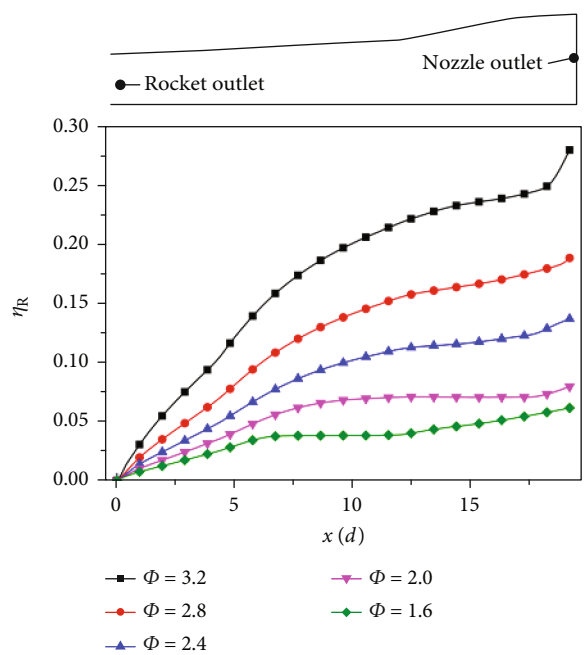

Figure 11: η_R distribution with different Φ conditions ($Ma_f = 0.9$).

3.2.2. Combustion Analysis. In the ejector mode, combustion mainly occurs in the mixing layer of the rocket plume and captured air. The combustion characteristics of the mixing layer directly affect the performance gain. The reaction efficiency and intensity are introduced to measure and quantify the combustion characteristics. The reaction efficiency (η_R) [10] represents the ratio of the total fuel consumption from the exit section of the rocket to any section and the fuel injection at the exit of the rocket, representing the fuel consumption rate along the flow direction. The reaction intensity (α) represents the fuel consumption of any axial distance (dx), representing the fuel consumption rate along the flow direction. α is a form of quantification of the heat release rate in the flow field. The greater the α is, the stronger the heat release. The expressions of the above two parameters are as follows:

$$\eta_R = \frac{\left(\int \rho u Y_{\text{fuel}} dA\right)_{\text{rkt}} - \int \rho u Y_{\text{fuel},x} dA}{\left(\int \rho u Y_{\text{fuel}} dA\right)_{\text{in}}},$$
$$\alpha = \frac{d}{dx}\left(\int \rho u Y_{\text{fuel},x} dA\right). \tag{3}$$

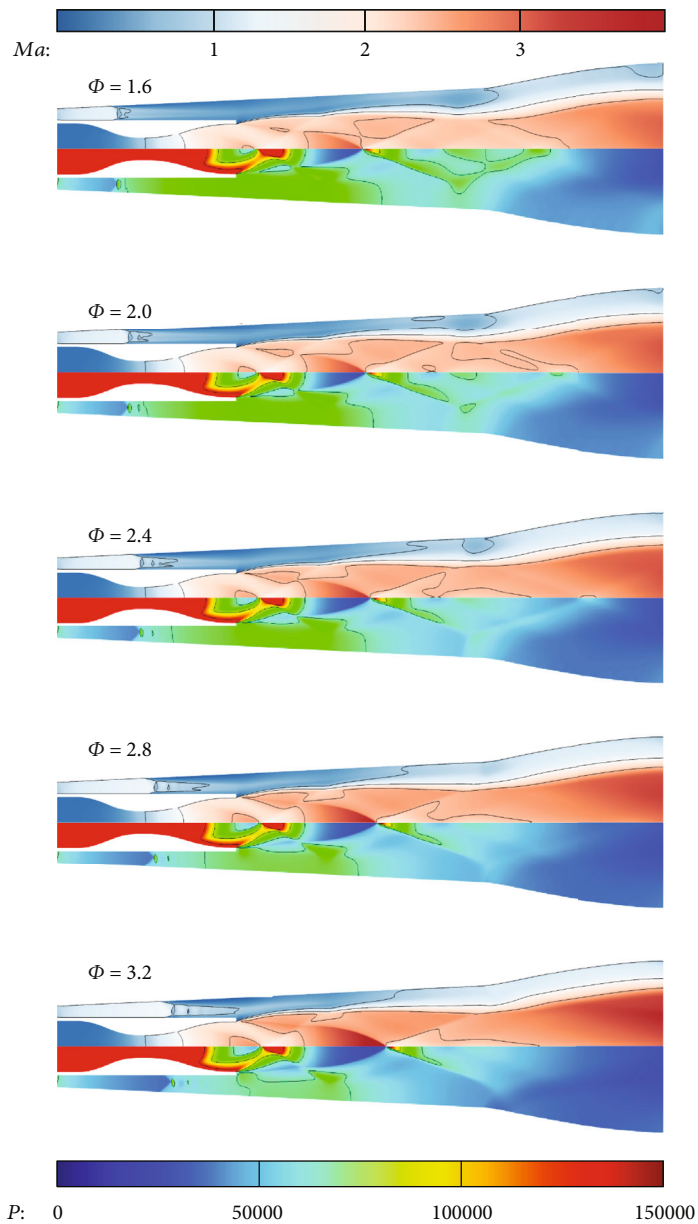

Figure 12: The cloud chart of Ma and P with different Φ conditions ($Ma_f = 1.8$).

Figure 9 shows cloud maps of M and H_r under different Φ conditions. With the increase of Φ, the mass fraction of fuel in the plume gradually decreases. Although $\dot{m}_{air}/\dot{m}_{rkt}$ gradually increases, due to the lack of fuel, the area of combustion and heat release gradually decreases. At $\Phi = 1.6$ and 2.0, it can be observed from the cloud maps of the heat release rate that the reacting mixing layer appears "wall impact" phenomenon. The rocket plume expands excessively in the combustor and hits the wall, called the "wall impact" phenomenon. With the $\Phi = 1.6$ condition, the "wall impact" point is at $x/d = 6.7$, and the "wall impact" point is at $x/d = 10.0$ with the $\Phi = 2.0$ condition. Figure 10 shows the change of α along the flow direction, which quantitatively characterizes the combustion heat release at different positions. At $\Phi = 1.6$, the heat release zone can be divided into three areas: initial reaction zone, "wall impact" zone, and rereaction zone. Near the exit of the rocket, the captured air contacted the rocket plume to react, which generates a large heat release and forms the initial reaction zone. Then, due to the expansion of the rocket plume, the mixing layer is squeezed into the wall in the combustor, and α in this area drops to 0, forming the "wall impact" zone. In the nozzle of RBCC, capture air and plume to reform reacting mixing layer, forming a heat release zone, namely, the rereaction zone.

The occurrence position of the "wall impact" phenomenon is the start point of the "wall impact" zone, and the start point of rereaction zone is the occurrence position of the flow separation (shown in Figure 7(a)). This shows that the reaction intensity has a great relationship with the flow characteristic of the RBCC engine. In addition, with a high fuel-rich degree, the α near the exit of the rocket is too high,

which is the main reason for the "wall impact" phenomenon. When $\Phi \geq 2.4$, the reacting mixing layers could never impact the wall, so there is no "wall impact" phenomenon in the reacting mixing layers. The curves of α distribution are continuous and raise at end of the RBCC nozzle because of the flow separation.

The "wall impact" phenomenon appears under the $\Phi = 1.6$ and 2.0 conditions, the kerosene mass fraction in the rocket plume is high, and α of the initial reaction zone is high, which leads to more heat release in the reacting mixing layer, thus reducing the eject performance of the rocket plume. The eject performance decreases, the mass flow of the captured air decreases, and the rocket plume expands more seriously, which eventually leads to the "wall impact" phenomenon. On the one hand, the "wall impact" phenomenon would cause the reaction to stop, on the other hand, it could increase the wall heat flow in the wall impact area and improve the difficulty of heat prevention. Figure 11 shows the curves of reaction efficiency (η_R) along the flow direction. It can be seen that with the increase of Φ, η_R is greatly improved. The low fuel-rich degree can make fuel consumption more sufficient.

In RBCC engines, under subsonic conditions, due to the low kinetic energy of captured air, the $\dot{m}_{air}/\dot{m}_{rkt}$ is mainly affected by the eject performance, and the I_{sp} of the RBCC engine is low. The "negative thrust effect" and "wall impact" phenomenons occur in the RBCC engine, which is not conducive to efficient operation. With a high fuel-rich degree, the "negative thrust effect" becomes weak, and the "wall impact" phenomenon would be enhanced. By singly adjusting the mixing ratio, the performance of the RBCC system cannot be effectively improved.

3.3. Flow Characteristics under the Supersonic Condition. With the increase of Ma_f, the advantages of high kinetic energy gradually appear. Figure 12 shows a cloud chart of Ma and P with different Φ conditions. The flow-choking phenomenon in the inlet of the isolator can be clearly observed. At the same time, with the increase of Φ, the position of flow choking gradually moves downstream, indicating that the eject performance of the plume is also gradually enhanced. It shows that the rocket plume with a low fuel-rich degree has stronger eject performance under both subsonic and supersonic conditions, combined with the flow of captured air basically remaining unchanged (shown in Figure 6) and the flow-choking phenomenon (shown in Figure 12) when $Ma_f = 1.8$. It can be concluded that at high Ma conditions, the main effect of the captured air is the geometric size. In the design of the RBCC engine, in order to ensure the system performance as much as possible, the inlet diameter is generally expected to be large. However, if the performance requirements under the ramjet and scramjet modes should be considered, there is an optimization and compromise process for the size design of the inlet.

The pressure distribution curves with different Φ conditions are shown in Figure 13. Due to the reaction between fuel in the rocket plume and air, the pressure in the combustor increases, especially with $x/d = -5 \sim 5$ area. As the corresponding H_f increases at high Ma_f, the ambient back pressure (P_a) decreases to 20.7 kPa. With the increase of fuel-rich degree, the heat release area of the reaction expands, and the overall heat release also increases. Because of the high kinetic energy of the captured air, the mix and combustion become more efficient in the combustor. Mixed flow still has high P after the expansion and acceleration of the nozzle, thus counteracting the effect of P_a, and the impact of " negative thrust surface" gradually weakens. Macroscopically, the specific impulse performance is significantly improved compared with under the subsonic condition.

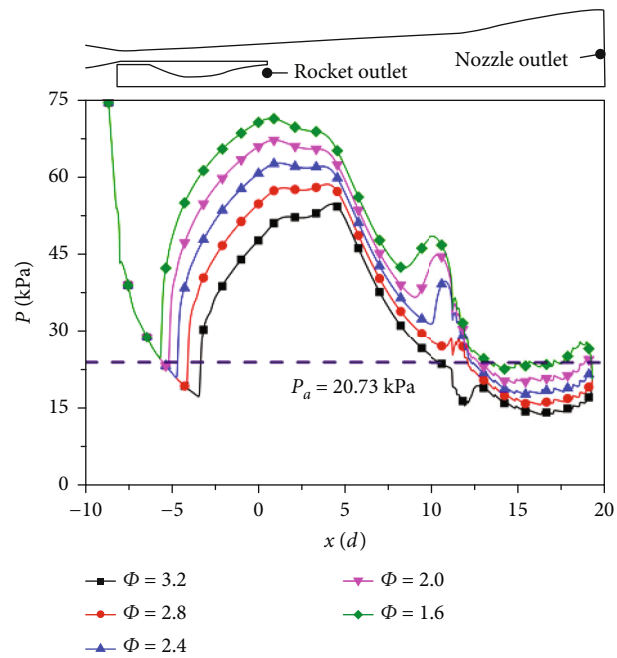

Figure 13: Pressure distribution with different Φ conditions ($Ma_f = 1.8$).

Figure 14 shows the change of M and H_r with different Φ conditions. Different from under the subsonic condition ($Ma_f = 0.9$), no matter how Φ changes, the area of H_r is continuous throughout the flow field under the supersonic condition ($Ma_f = 1.8$), and there is no "wall impact" phenomenon. Figure 15 shows α distribution with different Φ conditions. Obviously, it is hardly observed the "wall impact" zone ($\alpha = 0$). With the increase of Φ, the fuel available for combustion gradually decreases, and α remains at a low level, which is highly consistent with the cloud chart of H_r in Figure 14. The η_R distribution with different Φ conditions is shown in Figure 16. It can be concluded that the change rule of η_R is slightly similar to the low Ma_f situation, and the difference is that without the "wall impact" phenomenon, the reaction efficiency shows an increasing trend. At the nozzle outlet, when the $\Phi = 1.6$, 2.0, 2.4, 2.8, and 3.2, the η_R reaches 12.0%, 15.0%, 18.5%, 23.0%, and 29.2%, respectively. Due to the low efficiency of the reacting mixing layer, the rocket plume with the high fuel-rich degree has more unreacted fuel. In addition, due to the better combustion organization of captured air and rocket plume under high M_{af} conditions, the reaction efficiency is also higher than under low M_{af} conditions.

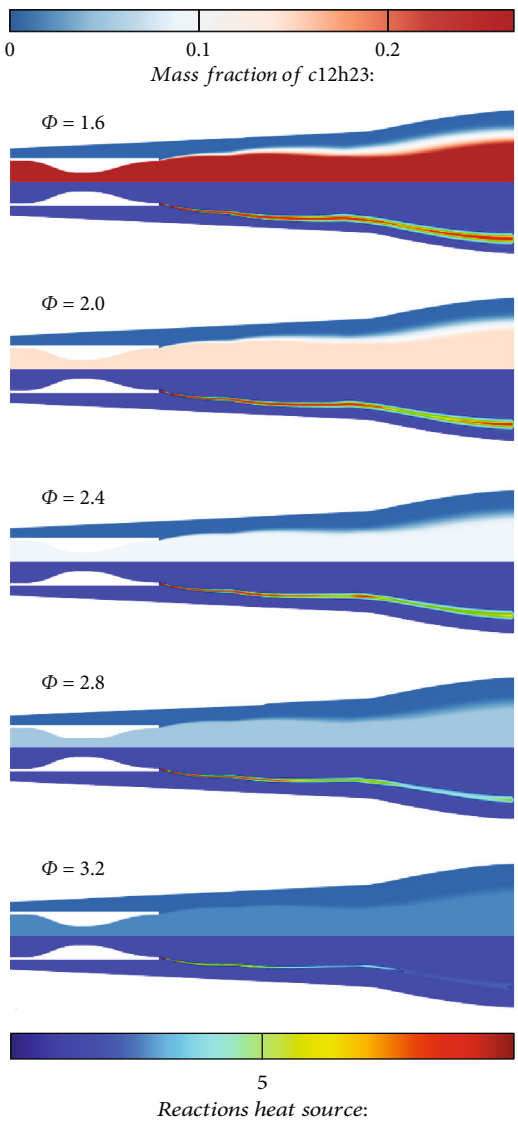

Figure 14: The cloud chart of M and H_r with different Φ conditions ($Ma_f = 1.8$).

Under supersonic conditions, the high fuel-rich degree can improve RBCC engine performance, but compared with the low fuel-rich degree, the reaction efficiency is lower, which indicates that the high fuel-rich degree would cause more fuel waste. Therefore, from the perspective of economy, it is not allowed to excessively improve the fuel-rich degree of the rocket to improve its performance.

4. Conclusions

Focusing on the critical technology of performance enhancement under the ejector mode, this paper undertakes a study on the performance of RBCC engines with varying rocket mixing ratios using the numerical simulation method. The research is aimed at drawing the main conclusions outlined below:

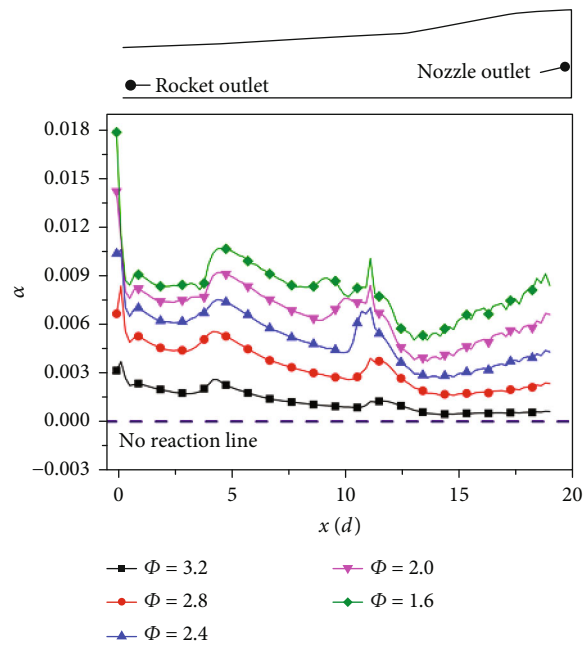

Figure 15: α distribution with different Φ conditions ($Ma_f = 1.8$).

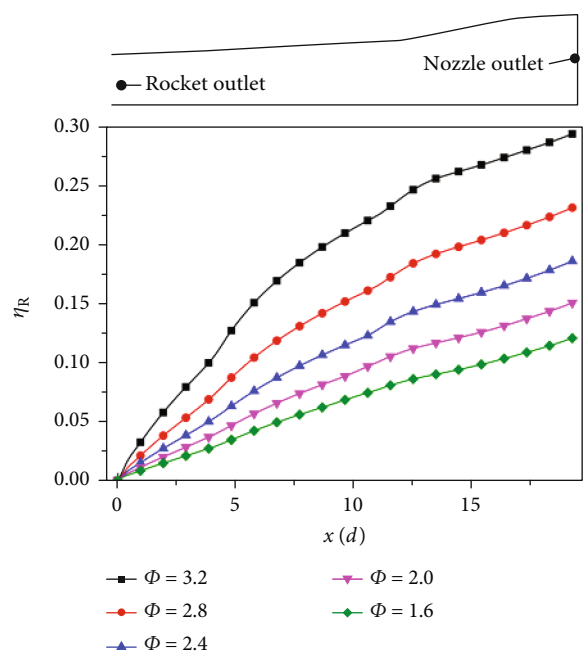

Figure 16: η_R distribution with different Φ conditions ($Ma_f = 1.8$).

(1) When the flight Mach number is low, enhancing the overall performance (I_{sp}) of the RBCC engine through adjustments in the rocket plume's mixing ratios becomes challenging. Conversely, under high flight Mach number conditions, the kinetic energy of the captured air increases, and improved overall performance (I_{sp}) of the RBCC engine can be achieved with a high fuel-rich degree in the rocket plume. Due to geometric constraints, altering the

ejector performance caused by mixing ratios becomes difficult and does not significantly impact the mass flow of captured air

(2) Under the subsonic condition ($Ma_f = 0.9$), with the low kinetic energy of the captured air, the RBCC engine may have the "negative thrust surface" and "wall impact" phenomena, inhibiting efficient and stable operation. The low fuel-rich degree could enhance the "negative thrust surface" phenomenon and weaken the "wall impact" phenomenon. Therefore, It is difficult to improve the performance of the RBCC engine by adjusting the mixing ratios alone. When the flight Mach number is low, it is an ideal strategy to adopt a low fuel-rich degree, with the help of nozzle adjustable technology to inhibit "negative thrust surface"

(3) Under the supersonic condition ($Ma_f = 1.8$), with the high kinetic energy of the captured air, the combustion organization in the combustor is better, and there is no "wall impact" phenomenon in the RBCC engine. When the fuel-rich degree is high, the RBCC engine can run efficiently. However, a high fuel-rich degree would cause more fuel waste, and a too-high fuel-rich degree will affect the working state of the rocket. When the flight Mach number is high, the RBCC engine can increase the fuel-rich degree to improve the overall performance to a certain extent

Data Availability

The data used to support the findings of this study are available from the corresponding authors upon request.

Conflicts of Interest

The authors declare that they have no known competing financial interests or personal relationships that could have appeared to influence the work reported in this paper.

Acknowledgments

This research work was supported by the National Natural Science Foundation of China (Grant No. 11925207).

References

[1] L. Shi, G. Zhao, Y. Yang et al., "Research progress on ejector mode of rocket-based combined-cycle engines," *Progress in Aerospace Sciences*, vol. 107, pp. 30–62, 2019.

[2] R. S. Fry, "A century of ramjet propulsion technology evolution," *Journal of Propulsion and Power*, vol. 20, no. 1, pp. 27–58, 2004.

[3] L. Shi, G. He, P. Liu et al., "A rocket-based combined-cycle engine prototype demonstrating comprehensive component compatibility and effective mode transition," *Acta Astronautica*, vol. 128, pp. 350–362, 2016.

[4] Y. Jia, W. Ye, P. Cui, and W. Xu, "Climbing performance analysis of rocket-based combined cycle engine powered aircraft," *Acta Astronautica*, vol. 162, pp. 135–144, 2019.

[5] L. M. Smith and S. L. Woodruff, "Renormalization-group analysis of turbulence," *Annual Review of Fluid Mechanics*, vol. 30, no. 1, pp. 275–310, 1998.

[6] P. G. Huang, P. Bradshaw, and T. J. Coakley, "Skin friction and velocity profile family for compressible turbulentboundary layers," *AIAA Journal*, vol. 31, no. 9, pp. 1600–1604, 1993.

[7] A. Kothari, J. Livingston, C. Tarpley, V. Raghavan, K. Bowcutt, and T. Smith, "A reusable, rocket and airbreathing combined cycle hypersonic vehicle design for access-to-space," in *AIAA SPACE 2010 Conference & Exposition*, Anaheim, California, 2010AIAA.

[8] T. Kanda, K. Tani, and K. Kudo, "Conceptual study of a rocket-ramjet combined-cycle engine for an aerospace plane," *Journal of Propulsion and Power*, vol. 23, no. 2, pp. 301–309, 2007.

[9] R. W. Foster, W. J. D. Escher, and J. W. Robinson, "Studies of an extensively axisymmetric rocket based combined cycle (RBCC) engine powered single-stage-to-orbit (SSTO) vehicle," in *25th AIAA/ASME/SAE/ASEE Joint Propulsion Conference*, pp. 89–2294, AIAA, Monterey, California, 1989.

[10] Z. Dong, M. Sun, Z. Wang, J. Chen, and Z. Cai, "Survey on key techniques of rocket-based combined-cycle engine in ejector mode," *Acta Astronautica*, vol. 164, pp. 51–68, 2019.

[11] W. Huang, L. Yan, and J.-g. Tan, "Survey on the mode transition technique in combined cycle propulsion systems," *Aerospace Science and Technology*, vol. 39, pp. 685–691, 2014.

[12] C. Gong, B. Chen, and L. Gu, "Design and optimization of RBCC powered suborbital reusable launch vehicle," in *19th AIAA International Space Planes and Hypersonic Systems and Technologies Conference*, pp. 1–20, AIAA Aviation, Atlanta, GA, 2014.

[13] L. T. Work and V. W. Haedrich, "Performance of ejectors as a function of the molecular weights of vapors," *Industrial and Engineering Chemistry*, vol. 31, no. 4, pp. 464–477, 1939.

[14] E. L. Petersen, V. P. Roan, and J. N. Pfahler, "Experimental investigation of supersonic-primary dissimilar-fluid ejectors," in *28th Joint Propulsion Conference and Exhibit*, pp. 92–3793, AIAA, Nashville, TN, U.S.A, 1992.

[15] W. Yang, Y. Xiang, A. Fan, and H. Yao, "Effect of the cavity depth on the combustion efficiency of lean H_2/air flames in a micro combustor with dual cavities," *International Journal of Hydrogen Energy*, vol. 42, no. 20, pp. 14312–14320, 2017.

[16] K. Miller, W. Anderson, and C. Jos, "Ducted rocket with simultaneous mixing and combustion direct-connect testing," in *40th AIAA/ASME/SAE/ASEE Joint Propulsion Conference and Exhibit Fort Lauderdale*, Florida, 2004.

[17] T. Kanda and K. Kudo, "Conceptual study of a combined-cycle engine for an aerospace plane," *Journal of Propulsion and Power*, vol. 19, no. 5, pp. 859–867, 2003.

[18] D. Parkinson, M. Turner, and D. Wagner, "Mixing of supersonic streams," in *35th Joint Propulsion Conference and Exhibit AIAA*, pp. 99–2454, Los Angeles,CA,U.S.A, 1999.

[19] M. Koupriyanov and J. Etele, "Equivalence ratio and constriction effects on RBCC thrust augmentation," *Acta Astronautica*, vol. 68, no. 11-12, pp. 1839–1846, 2011.

[20] S. Han, J. Peddieson Jr., and D. Gregory, "Ejector primary flow molecular weight effects in an ejector-ram rocket engine," *Journal of Propulsion and Power*, vol. 18, no. 3, pp. 592–599, 2002.

[21] R. Gu, M. Sun, Z. Cai, P. Li, and Y. H. Huang, "Numerical modeling and experimental investigation on the rocket-

ejector system with limited mixer length," *Acta Astro-nautica*, vol. 182, pp. 13–20, 2021.

[22] R. Gu, *Investigation of Characteristics of Combustion Organizations and Mixing in an Axisymmetric Rocket-Based Combined-Cycle Engine Operating in Ejector Mode*, National University of Defense Technology, 2021.

[23] J. L. Hall, "Experimental investigation of structure, mixing and combustion in compressible turbulent shear layers," California Institute of Technology, 1991.

[24] N. D. Sandham and W. C. Reynolds, "Compressible mixing layer - linear theory and direct simulation," *AIAA Journal*, vol. 28, no. 4, pp. 618–624, 1990.

[25] S. Sarkar and B. Lakshmanan, "Application of a Reynolds stress turbulence model to the compressible shear layer," *AIAA Journal*, vol. 29, no. 5, pp. 743–749, 1991.